







Article

Hydrogeochemistry and Isotopic Composition of Waters in the Renella Cave (Central Italy): New Insights into Groundwater Dynamics

Marco Chimenti ^{1,*}, Stefano Natali ^{1,2,3} , Roberto Giannecchini ^{1,3,4} , Giovanni Zanchetta ^{1,4,5},
Ilaria Baneschi ³ , Marco Doveri ³ , Ilaria Isola ^{3,6}  and Leonardo Piccini ^{2,7} 

¹ Department of Earth Sciences, University of Pisa, 56126 Pisa, Italy; stefano.natali@unifi.it (S.N.); roberto.giannecchini@unipi.it (R.G.); giovanni.zanchetta@unipi.it (G.Z.)

² Department of Earth Sciences, University of Florence, 50121 Florence, Italy; leonardo.piccini@unifi.it

³ Institute of Geosciences and Earth Resources, IGG-CNR, 56124 Pisa, Italy; ilaria.baneschi@igg.cnr.it (I.B.); marco.doveri@igg.cnr.it (M.D.); ilaria.isola@ingv.it (I.I.)

⁴ Centre for Climatic Change Impact, CIRSEC, University of Pisa, 56124 Pisa, Italy

⁵ Institute of Environmental Geology and Geoengineering, IGAG-CNR, Montelibretti, 00015 Rome, Italy

⁶ Istituto Nazionale di Geofisica e Vulcanologia, INGV, 56100 Pisa, Italy

⁷ Commissione Scientifica—Federazione Speleologica Toscana, 57120 Livorno, Italy

* Correspondence: marco.chimenti@phd.unipi.it

Abstract: This article presents data from monthly monitoring carried out on cave and stream waters belonging to the Renella Cave karst system from September 2020 to April 2022. Additionally, old data pertaining to cave waters from previous published work are discussed. The aim is to develop a dataset for future climatic and hydrological studies on the Renella Cave and its surface recharges. Water samples were collected and analyzed for major ions, $\delta^{18}\text{O}$ and $\delta^2\text{H}$, on water molecules. The cave sump water level, water temperature, and electrical conductivity were continuously measured and compared to the precipitation data. Additionally, air temperature and pressure inside and outside the cave were also monitored. The classification based on the Piper-Hill diagram indicated that both stream and cave waters belong to the bicarbonate-alkaline earth hydrochemical facies, indicating that their chemism is essentially determined by the dissolution of the Grezzoni Fm. Isotopic data suggest that both stream and cave waters have a meteoric origin, and their variability mainly depends on underground homogenization. Hydrogeochemistry, isotopic composition, and the monitoring data allowed a deeper understanding of the cave karst system, and identified an underground circulation network that is fragmented into independent parts.

Keywords: hydrological monitoring; karst system; Apuan Alps; hydrogeochemistry; stable isotopes



Citation: Chimenti, M.; Natali, S.; Giannecchini, R.; Zanchetta, G.; Baneschi, I.; Doveri, M.; Isola, I.; Piccini, L. Hydrogeochemistry and Isotopic Composition of Waters in the Renella Cave (Central Italy): New Insights into Groundwater Dynamics. *Water* **2023**, *15*, 1764. <https://doi.org/10.3390/w15091764>

Academic Editor: Hucai Zhang

Received: 11 April 2023

Revised: 27 April 2023

Accepted: 2 May 2023

Published: 4 May 2023



Copyright: © 2023 by the authors. Licensee MDPI, Basel, Switzerland. This article is an open access article distributed under the terms and conditions of the Creative Commons Attribution (CC BY) license (<https://creativecommons.org/licenses/by/4.0/>).

1. Introduction

Groundwater represents an important resource, exploited for agricultural, industrial, and many other human activities [1–4], and it accounts for ~98% of the Earth's available fresh water [5]. Karst groundwater is one of the most important sources of the drinking water supply and serves approximately 25% of the world's population [6–12]. Karst aquifers represent significant water reservoirs, both in terms of quality and water volumes that could potentially be stored, and they often feed large, tapped springs [4]. Hence, the over-exploitation of these groundwater resources due to human activities is a global issue [13] and is further emphasized by climate change that modifies the hydrological cycle [14,15]. Investigation on karst groundwater is challenging due to significant karstification that determines distinctive heterogeneity and anisotropy of the aquifer's hydraulic properties [16,17]. The high effective infiltration rates and high flow velocities determine the rapid transfer of recharging waters into karst systems with very short water residence times, which results in their high vulnerability [18]. The high variability of karst groundwater flows in space

and time [19,20], which makes understanding and modelling karst groundwater circulation even more difficult. Moreover, direct investigations and measurements of hydrodynamic and hydrochemical features of groundwater in karst environments are often limited to the sampling of natural springs and/or cave waters.

For these reasons, karst caves represent optimal sites to investigate the water flows from the surface through the epikarst and vadose zone to the phreatic environment, thus attempting to reconstruct the circulation pattern of groundwater, assessing its availability, quality, residence times, and estimating the contribution of infiltration to the karst system recharge [21–23].

In this paper, we provide insights into the chemical and isotopic composition and hydrodynamics of groundwater flowing through the Renella Cave, a small cave located in the northern Apuan Alps. This cave has recently been studied for paleoclimatic and paleoenvironmental reconstructions [24–29], and the present work aims to characterize water flowing within this karst system as a background for future research. For this purpose, new hydrodynamic, chemical, and isotopic data on the cave sump waters from two-year monitoring are presented and discussed together with previously published data [27,28]. Surface waters were also sampled, and meteorological conditions inside and outside the cave were monitored.

2. Study Area

2.1. Geomorphological and Geological Setting

The Apuan Alps is a mountain range spreading over an area of about 650 km² in northwestern Tuscany (Central Italy). The chain is NW–SE oriented and runs parallel to the coastline, which is separated by a long and narrow plain area known as the Apuo-Versilia Plain (Figure 1a) and reaches a maximum elevation of 1942 m a.s.l. at Mt. Pisanino.

The Apuan Alps represent one of the most important karst areas in Italy and Europe, and they host large volumes of groundwater resources within metamorphic and non-metamorphic carbonate aquifers [4,30]. According to [4], these aquifers are highly karstified due to physical–chemical processes, and the superficial fracturing is responsible for high rates of rainfall infiltration. These conditions imply a high hydraulic conductivity, thus emphasizing the transfer of surface waters to groundwater. Several springs are fed by karst aquifers [4,31], and most of them drain metamorphic carbonate aquifers and supply drinking water for the inhabitants of the Apuan Alps and surrounding areas [4]. The highly karst character of aquifers in the Apuan Alps area is clearly depicted by the presence of about 1200 known karst caves [4], with the overall cave system extending for over 325 km. Most of these caves develop within carbonate formations of metamorphic units, especially metadolomite and marble (“Grezzoni”, Marmi Dolomitici, and Marmi Fm.).

The Renella Cave (44.09500, 10.18361) is a small shallow cave located in the northernmost sector of the Apuan Alps, about 1.5 km upstream of the village of Forno (Figure 1a,b). The cave is placed in a narrow valley at the confluence of the Regolo Creek and the Frigido River (here named Secco Creek due to the absence of surface flow for most of the year) (Figure 1a,b). The cave has only one entrance (artificially modified) (Figure 2b) at an altitude of 275 m a.s.l. on the right side of the Frigido River valley on the western side of the Apuan Alps (Figure 2a), upstream of the Frigido River spring (Forno Spring, Figure 1b). The cave has a predominantly horizontal development for a total length of ca. 200 m, and it extends vertically for ca. 23 m. It develops within a Triassic dolomite (Grezzoni Fm.), close to the contact with the Palaeozoic phyllitic basement [29]. The metadolomite beds dip almost vertically, and the cave development follows the WSW–ENE direction of the strike [27]. The cave probably has a phreatic origin, being the marginal part of an extensive epiphreatic system which was affected by the invasion of alluvial sediments once it was intercepted by surface stream incision during a recent phase of downcutting [29]. It exhibits evidence of a complex hydrodynamic evolution and presently experiences a dual hydrological function [29]. The former is a subterranean shortcut for the Regolo Creek via a stream sink, which is currently buried by streambed deposits; the latter reasonably plays as

an occasional overflow spring for the local karst aquifer, whose major outflow is the Forno Spring, with a mean flow rate of about 1.6 m³/s [32].

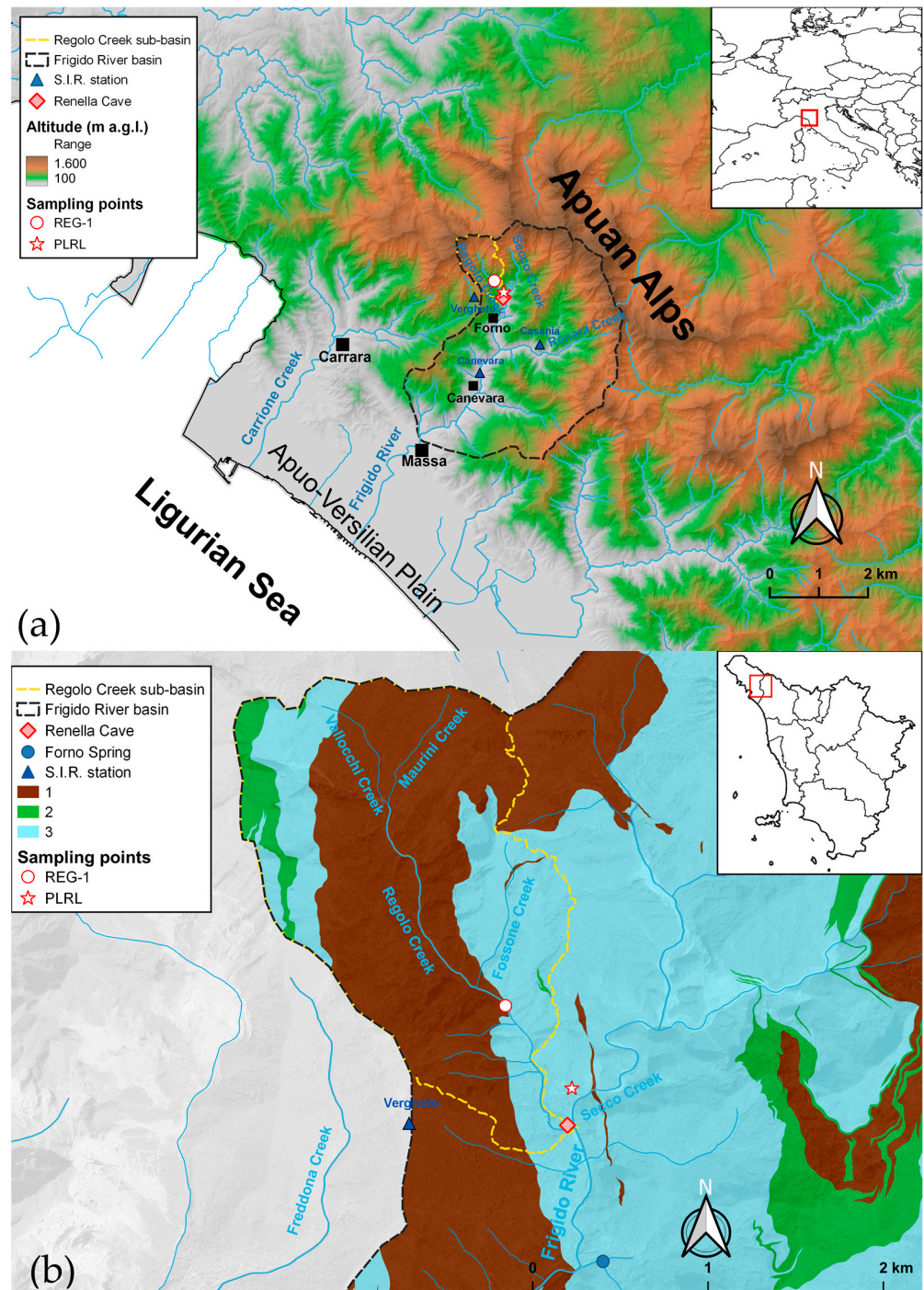


Figure 1. (a) Map of the study area. Location of the Renella Cave, sampling points, and S.I.R. stations. (b) Hydrogeological sketch map of the study area. 1—metacarbonate rocks with high permeability (mainly Grezzoni Fm. and marble). 2—metacarbonate rocks with medium permeability (Metalcari Selciferi Fm. and Entrochi metalimestone). 3—non-carbonate rocks with low permeability (mainly Porfiroidi e Scisti porfirici Fm. and phyllite).

Several active speleothems are present, mostly represented by stalactites, stalagmites, and flowstones, some of which have been sampled since the early 2000s for paleoclimatic

and paleohydrological studies, e.g., [24–29]. Moreover, the lower part of the cave is frequently flooded through a small cave sump.

The natural environment around the cave is heavily modified by human activity since an abandoned dolostone quarry is located just upstream of the cave (Figure 2c). The quarry (called Cava Serroni) has been in a state of abandonment since 1999, as no securing and restoration activities have been carried out so far. The buildings and plants have not been dismantled; the scraps have not been removed. The company holding the quarrying concession was also responsible for the removal of a rocky ridge on the left side of the Regolo Creek, carried out to open an easier access to the quarry. Consequently, during very rainy periods, part of the water falls into the quarry from a height of over 100 m. This implies an intense washout of sludges accumulated in the quarry yards, which may easily infiltrate the underlying karst aquifer by means of meteoric waters, enhancing the vulnerability of the groundwater resources [24,32]. The soil is almost absent or poorly developed above the cave, mainly due to the large presence of carbonate rocks and the high slope.

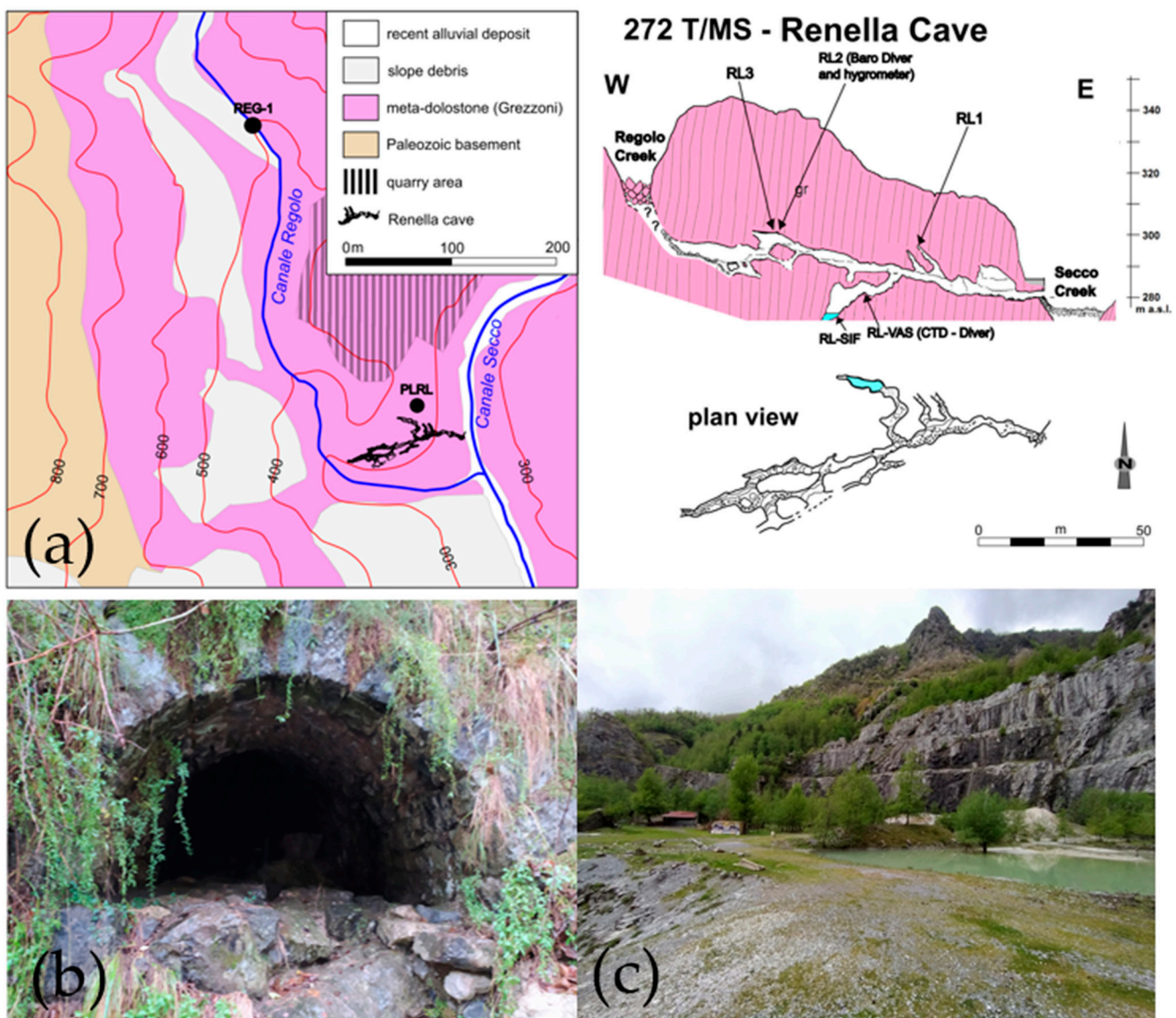


Figure 2. (a) Map of the Renella Cave, geological sketch map of the study area, and location of sampling points and monitoring instruments (modified from [29]). (b) Entrance of the Renella Cave. (c) Quarry area above the Renella Cave.

2.2. Local Climate

According to Köppen's classification system [33], the climate in the Renella Cave area can be referred to as Csb. The Apuan Alps prevalently receives its rainfall from the arrival of Atlantic frontal air masses [34] which interact often with the most important cyclogenetic center of the Western Mediterranean area, the Gulf of Genoa [35,36]. In this context, the Apuan Alps reliefs act as an orographic barrier to air masses moving eastward, thus triggering local cyclogenesis [37]. According to this framework, the autumn/winter precipitation patterns over northwestern Tuscany are influenced by the North Atlantic Oscillation (NAO) teleconnection [38,39], as indicated by the negative correlation between the NAO index and the rainfall amount [28,39]. The Apuan Alps experience a Mediterranean climate with a marked North Atlantic influence [35,38,39]. The proximity to the sea and the peculiar orography of the Apuan Alps chain, characterized by steep slopes, induce the lifting of humid air masses and their rapid adiabatic cooling, thus producing high precipitation that locally exceeds 3000 mm/year [4,37,40].

According to the literature [25,27–29], the temperature inside the Renella Cave is quite constant at ca. 13 °C, while the mean monthly temperatures for the surrounding area range from a minimum of 7.4 °C in January to a maximum of 23.1 °C in July. The mean annual total precipitation is about 2020 mm (± 410 mm) over the Renella Cave area, as calculated using the instrumental time series measured from 1927 to 1999 (except for some short breaks) at the closest meteorological station (Casania—TOS10000050; Figure 1a) of the regional hydrologic service (<http://www.sir.toscana.it/pluviometria-pub> (accessed on 1 May 2022)) about 3 km away.

3. Materials and Methods

3.1. Samples Collection

Sporadic monthly sampling of cave drips, a drip pool, and the cave sump was carried out during the 2009–2013 period for hydrochemistry and isotope analysis. Two systematic monitoring of three drips, the drip pool, and the sump were also performed from March 2015 to March 2016 [41,42], and samples were analyzed for both chemical and isotopic composition. Samples were collected from three drips (named RL1, RL2, and RL3) placed in different cave sectors. RL1 is located in the first sector of the cave, quite close to the entrance, where the minimum thickness of rock cover occurs. RL2 and RL3 are located in the inner sector of the cave, quite close to the inlet point of the Regolo Creek as also proven by the occurrence of alluvial sediments [29]. A monthly integrated sampling plan was established for the three monitored drips. Double-sealing HDPE bottles with a volume of 125 mL were used to collect drip waters at RL1 and RL2, whereas 500 mL bottles were used at RL3. Different bottles were used for drips because of different drip rates among RL1, RL2, and RL3, even though no direct drip rate measurements were performed. Water samples from the cave sump (named RL-SIF) and the drip pool (named RL-VAS) were also collected in double-sealing HDPE bottles with different aliquots, including 125 mL “as is” for major anion analysis (Cl^- , NO_3^- , SO_4^{2-}), 50 mL filtered through 0.45 μm cellulose acetate filters and acidified with ultrapure HNO_3 for major cations analysis (Na^+ , K^+ , Ca^{2+} , and Mg^{2+}), and 50 mL filtered for isotopic analysis ($\delta^{18}\text{O}$ and $\delta^2\text{H}$).

The new systematic monitoring was carried out from September 2020 to April 2022. Samples were collected monthly from the drip pool (until April 2021), cave sump, and Regolo Creek (named REG-1). Monthly precipitations were also collected from November 2020 to March 2022 using a homemade rain gauge (named PLRL) placed at about 315 m a.s.l. quite close to the cave entrance. Part of the precipitation data has already been published in [37], in which sampling procedures are reported. These data are used in this work as an isotopic benchmark for precipitation in the study area. Water samples from the drip pool, cave sump, and Regolo Creek were collected in double-sealing HDPE bottles with different aliquots as for RL-SIF and RL-VAS.

3.2. Field Measurements

Water temperature (T ; °C), pH, and electrical conductivity (EC; $\mu\text{S}/\text{cm}$ at 25 °C) of the cave sump, drip pool, and Regolo Creek waters were measured in the field using portable waterproof instruments (XS Instruments). Total alkalinity (totally attributable to HCO_3^- , given the pH values) was also determined in situ by acidimetric titration with 0.1 N HCl using methyl-orange as an indicator. Water temperature, electrical conductivity, and pH accuracy was 0.25% for temperature, 0.5% for conductivity, and 0.1 for pH. The pH and EC sensors were calibrated prior to each sampling trip with certified standard buffer solutions of pH 4, 7, 10, and 1413 $\mu\text{S cm}^{-1}$ solutions, respectively. The error of the alkalinity analysis was 0.01 meq L^{-1} , tested in laboratory with certified bicarbonate solutions. Flow rate measurements of the Regolo Creek were carried out during five field samplings (November 2020–May 2021) using the salt dilution method [43,44].

Two automatic probes were placed in the inner sector of the Renella Cave to measure the cave temperature (T_{cave}), atmospheric pressure, and relative humidity (RH). A Baro-Diver probe (Schlumberger Water Services) was placed within the cave close to RL2 on 1 September 2020, to measure the cave temperature with an accuracy of ± 0.1 °C and a resolution of 0.01 °C, and the atmospheric pressure with an accuracy of ± 0.5 cmH_2O . A Tinytag Plus 2 Logger (Gemini Data Loggers) with temperature and RH probe was used to monitor the relative humidity inside the cave over the monitoring period. The measurement range of this probe was between 0 and 100% with an accuracy of $\pm 3.0\%$ RH readings at 25 °C and a resolution better than 0.3% RH readings. However, the working range for the RH probe depends on relative humidity/temperature limits, with performance tending to deteriorate as the temperature increases and for RH values very close to 100%. The probe was placed on 30 April 2021, and it has been working until 19 November 2021. After this date, the instrument experienced a progressive drift toward lower values, probably due to the high RH values inside the cave (close to 100%) which likely caused damages to the measurement probe. The atmospheric temperature (T_{atm}) was also monitored outside the cave using another Baro Diver probe that was placed in the quarry yard above the cave, very close to the rain gauge used to collect monthly precipitation.

In order to better understand the hydrodynamic and the processes behind physico-chemical variations of the cave sump, a CTD Diver probe (Schlumberger Water Services) was installed on 29 January 2021. Every five minutes, the probe registered the water temperature with an accuracy of ± 0.1 °C and a resolution of 0.01 °C, the water level in terms of water pressure with an accuracy of ± 0.5 cmH_2O and a resolution of 0.2 cmH_2O , and the EC with an accuracy of $\pm 1\%$ and a resolution of $\pm 0.1\%$ of readings.

3.3. Laboratory Analysis

The analysis of major elements was carried out at the Institute of Geosciences and Earth Resources of the National Research Council (IGG-CNR) of Pisa. Major anions were determined by ion chromatography (IC) using a Metrohm 883 Basic IC Plus. Major cations concentrations were obtained by inductively coupled plasma optical emission spectroscopy (ICP-OES) using a PerkinElmer Optima 2000TM DV. In every case, the relative standard deviation (RSD), calculated on three replicate injections, was $<10\%$. The charge balance error was used to ensure the accuracy of the analysis for major elements [45] and it was $<5\%$ for each sample. For major anions, the analyses included replicates, blanks, and quality-control standards measured with every set of unknown samples, the concentrations of which were calculated from daily calibration curves. Different analytical techniques were used to determine the oxygen and hydrogen stable isotope composition of water samples. The $^{18}\text{O}/^{16}\text{O}$ isotope ratios of samples collected before December 2020 were determined using an Isotope Ratio Mass Spectrometry (Thermo Finnigan MAT252, Thermo Fisher, Waltham, Massachusetts, USA) of gaseous CO_2 , previously equilibrated with water at 25 °C [46]. Hydrogen stable isotopes were measured using a Los Gatos Research Liquid Water Isotope Analyzer (LGR-LWIA) based on the “Off-Axis Integrated Cavity Output Spectroscopy” technique [47]. These analyses were also performed at the IGG-CNR of

Pisa. Samples collected in the period during 2021–2022 were analyzed in the Laboratory of Fluid Geochemistry of the University of Florence by using a Picarro L2130-i analyzer based on cavity ring-down spectroscopy (CRDS). The oxygen and hydrogen isotope data are expressed as $\delta\text{‰}$ compared to the international reference standard V-SMOW [48]. The analytical precision was 0.1‰ and 1‰ for $\delta^{18}\text{O}$ and $\delta^2\text{H}$ for all the adopted methods. All the laboratories ran isotopic reference materials spanning isotope scales of interest and calibrated them with internationally distributed isotopic reference materials obtained from IAEA to the VSMOW-SLAP scale. An internal lab standard was run several times among samples as a check on the instrumentation.

4. Results

4.1. Atmospheric and Cave Conditions

The raw data of the external temperature (T_{ext}) and cave temperature (T_{cave}) measured at PLRL and RL2, respectively, are shown in Figure 3.

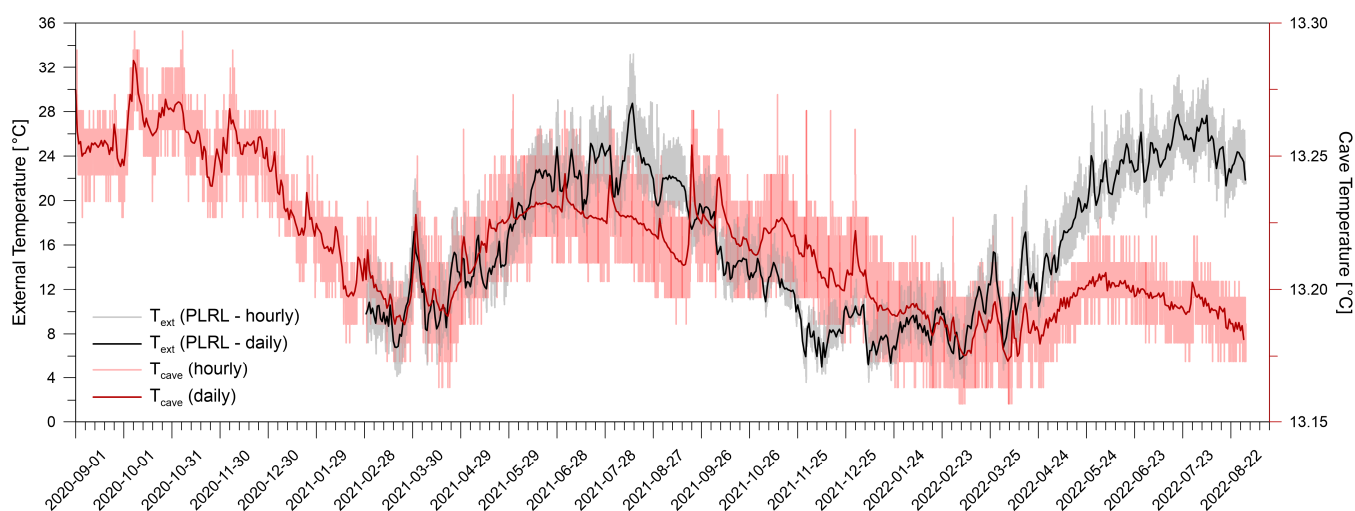


Figure 3. Hourly and daily data of external temperature (T_{ext}) and cave temperature (T_{cave}). Text was plotted on the left vertical axis, whereas T_{cave} was plotted on the right vertical axis.

The mean monthly atmospheric temperature outside the cave ranged from a minimum of 7.7 °C in January to a maximum of 23.3 °C in July, with a mean value of the monthly mean of 14.2 ± 5.8 °C. The mean cave air temperature over the monitoring period was 13.2 °C with a standard deviation of ± 0.03 °C, which was less than the instrument accuracy. The latter was very constant as indicated by the very low standard deviation (sd), and very close to the mean annual temperature for the studied area as reported by [29]. We also measured that the relative humidity inside the cave was always 100%, although the instrument error was $\pm 3\%$ and it worked poorly with high humidity values. Under these conditions, drip waters should not be subjected to evaporative isotopic fractionation during dripping. This has implications for the climatic significance of the $\delta^{18}\text{O}$ of drip waters, which is generally considered in this Mediterranean area as a proxy of paleoprecipitation [24–29,49,50]. The $\delta^{18}\text{O}$ of drip waters should faithfully reflect the $\delta^{18}\text{O}$ of precipitation, if evaporation does not occur in the epikarst and in the cave.

4.2. Physico-Chemical Parameters, Hydrogeochemistry of Stream and Cave Waters, and Hydrodynamic Conditions of the Cave Sump

The raw data of the physico-chemical parameters (EC, pH, and T) measured on the field of drips, drip pool, cave sump, and Regolo Creek are provided in the Supplementary Materials (SM—Table S1). The statistics for the field parameters of the waters are reported in Tables 1 and 2. The drip pool (RL-VAS) showed slightly variable pH values ranging from a minimum of 7.9 to a maximum of 8.2. The hydrogen ion concentration was a little more variable at the Regolo Creek (REG-1) and the cave sump (RL-SIF), with a pH ranging from

7.7 to 8.3 and from 7.8 to 8.2, respectively, indicating slightly alkaline conditions. During the entire monitoring period, the drip pool was characterized by a higher EC than the cave sump and Regolo Creek, which, on the opposite hand, showed similar trends, with slightly higher values in the sump. The EC varied from 375 to 454 $\mu\text{S}/\text{cm}$ for the drip pool, whereas lower values were registered in the cave sump and Regolo Creek, ranging from 244 to 154 $\mu\text{S}/\text{cm}$, and from 182 to 111 $\mu\text{S}/\text{cm}$, respectively. The drip pool temperature was the least variable, ranging from 12.2 to 13.2 $^{\circ}\text{C}$ due to the longer residence time that allowed the waters to thermally equilibrate with the cave temperature. The temperature of the creek varied within a large interval from a minimum of 3.9 to a maximum of 13.9 $^{\circ}\text{C}$, whereas the temperature of the cave sump was less variable, ranging from 10.2 to 12.4 $^{\circ}\text{C}$. The variations in the physico-chemical parameters of the cave sump and Regolo Creek waters were in agreement with the precipitation patterns, with higher values during periods characterized by total absence or scarcity of precipitation, and lower values when heavy rainfall occurred. The drip pool, on the other hand, showed variations that were very attenuated and not directly attributable to the precipitation regime.

Table 1. Statistical table of physico-chemical parameters, major ions, and isotope of water samples.

Parameter	Code	2020–2022				2015–2016					2009–2013				
		RL-SIF	RL-VAS	REG-1	PLRL	RL-SIF	RL-VAS	RL1	RL2	RL3	RL-SIF	RL-VAS	RL1	RL2	RL3
	<i>n</i>	7	8	8	/	7	9	5	9	/	3	4	/	/	/
T ($^{\circ}\text{C}$)	min	10.2	10.8	3.9	/	9.2	11.4	/	/	/	9.2	11.4	/	/	/
	mean	11.1	12.3	10.1	/	11.7	12.9	/	/	/	10.9	12.4	/	/	/
	sd	0.8	0.7	4.8	/	1.1	0.6	/	/	/	1.6	0.7	/	/	/
	max	12.4	13.2	19.9	/	13.3	13.5	/	/	/	12.3	12.9	/	/	/
pH	min	7.9	8.1	7.6	/	7.6	7.9	/	/	/	8.1	8.3	/	/	/
	mean	8.1	8.3	8.1	/	8.0	8.2	/	/	/	8.1	8.3	/	/	/
	sd	0.1	0.1	2.6	/	0.2	0.2	/	/	/	0	0	/	/	/
	max	8.2	8.4	8.4	/	8.2	8.4	/	/	/	8.2	8.4	/	/	/
EC ($\mu\text{S}/\text{cm}$ at 25 $^{\circ}\text{C}$)	min	154	322	111	/	143	290	/	/	/	143	357	/	/	/
	mean	182	391	156	/	175	387	/	/	/	162	393	/	/	/
	sd	25	39	32	/	24	40	/	/	/	31	40	/	/	/
	max	244	454	224	/	204	444	/	/	/	198	444	/	/	/
HCO ₃ (mg/L)	min	73.2	207.5	47.0	/	76.3	195.0	142.0	142.0	/	75.1	140.3	/	/	/
	mean	94.1	258.0	75.4	/	95.4	254.8	148.0	150.0	/	90.7	230.7	/	/	/
	sd	23.9	30.2	17.1	/	14.4	30.5	4.0	5.0	/	27.1	62.7	/	/	/
	max	140.3	294.7	103.7	/	114.0	289.0	154.0	159.0	/	122.0	273.4	/	/	/
Cl (mg/L)	min	5.9	5.3	4.9	/	4.9	5.1	3.9	4.1	/	5.3	0.9	/	/	/
	mean	6.9	5.8	5.6	/	5.9	5.4	4.4	4.7	/	5.8	5.4	/	/	/
	sd	1.0	0.6	0.6	/	0.9	0.2	0.5	0.3	/	0.7	3.1	/	/	/
	max	8.6	7.2	6.4	/	7.6	5.6	5.1	5.0	/	6.5	7.6	/	/	/
SO ₄ (mg/L)	min	4.0	5.0	3.1	/	4.2	4.9	1.0	1.0	/	4.8	1.7	/	/	/
	mean	4.9	6.1	5.0	/	5.7	6.2	1.3	1.1	/	6.2	7.8	/	/	/
	sd	1.2	0.9	1.3	/	0.8	0.6	0.2	0.1	/	2.1	4.7	/	/	/
	max	7.4	7.6	7.0	/	6.5	7.1	1.6	1.3	/	8.7	12.9	/	/	/
NO ₃ (mg/L)	min	0.6	0.4	0.1	/	2.0	1.0	2.2	3.7	/	1.2	1.2	/	/	/
	mean	1.7	0.7	0.3	/	2.8	1.3	2.4	4.4	/	1.8	1.2	/	/	/
	sd	1.0	0.2	0.1	/	0.7	0.1	0.1	0.4	/	0.7	0	/	/	/
	max	3.5	0.9	0.4	/	3.9	1.4	2.5	4.8	/	2.6	1.2	/	/	/
Na (mg/L)	min	3.3	3.1	2.7	/	3.2	3.4	2.7	3.2	/	3.5	0.8	/	/	/
	mean	3.8	3.3	3.2	/	4.4	3.7	2.9	3.7	/	3.9	3.4	/	/	/
	sd	0.5	0.2	0.3	/	0.9	0.4	0.1	0.7	/	0.7	1.7	/	/	/
	max	4.6	3.6	3.5	/	5.8	4.6	3.0	5.6	/	4.7	4.5	/	/	/
K (mg/L)	min	0.5	0.3	0.1	/	0.4	0.3	0.1	0.1	/	0.3	0.1	/	/	/
	mean	1.1	0.7	0.2	/	0.9	0.4	0.1	0.1	/	0.4	0.3	/	/	/
	sd	0.4	0.6	0.0	/	0.4	0.1	0.0	0.0	/	0.1	0.1	/	/	/
	max	1.4	2.2	0.3	/	1.6	0.5	0.1	0.1	/	0.5	0.5	/	/	/
Ca (mg/L)	min	16.0	29.0	11.6	/	16.8	22.8	25.7	24.6	/	16.1	29.1	/	/	/
	mean	17.8	37.2	18.0	/	19.4	35.8	26.8	26.5	/	18.3	35.4	/	/	/
	sd	1.5	5.6	3.8	/	1.3	7.4	0.7	0.9	/	2.1	6.5	/	/	/
	max	20.4	43.9	22.5	/	20.7	43.5	27.6	27.5	/	20.1	43.2	/	/	/

Table 1. *Cont.*

Parameter	2020–2022					2015–2016					2009–2013				
	Code	RL-SIF	RL-VAS	REG-1	PLRL	RL-SIF	RL-VAS	RL1	RL2	RL3	RL-SIF	RL-VAS	RL1	RL2	RL3
	<i>n</i>	7	8	8	/	7	9	5	9	/	3	4	/	/	/
Mg (mg/L)	min	6.4	28.1	3.7	/	6.0	26.7	12.6	14.0	/	6	29.2	/	/	/
	mean	9.3	30.2	4.9	/	9.0	30.8	13.6	14.6	/	8.4	31.6	/	/	/
	sd	3.1	1.2	0.9	/	2.3	2.4	0.7	0.5	/	3.7	2.9	/	/	/
	max	15.0	31.8	6.1	/	12.1	34.9	14.4	15.2	/	12.7	35	/	/	/
	<i>n</i>	13	17	10	17	7	9	5	9	7	3	4	2	2	2
$\delta^{18}\text{O}$ (‰)	min	−8.21	−6.01	−35.95	−9.68	−6.85	−6.65	−6.49	−6.63	−6.67	−7.11	−6.29	−6.46	−6.26	−6.72
	mean	−6.29	−5.77	−34.95	−5.56	−6.49	−6.28	−6.32	−6.47	−6.5	−6.85	−5.96	−6.28	−6.23	−6.45
	sd	0.88	0.12	0.69	2.20	0.29	0.18	0.23	0.09	0.15	0.23	0.28	0.25	0.04	0.39
	max	−5.03	−5.55	−34.00	−1.75	−6.08	−6.08	−5.94	−6.32	−6.32	−6.70	−5.63	−5.94	−6.20	−6.17
$\delta^2\text{H}$ (‰)	min	−50.1	−36.0	−52.6	−62.9	−43.7	−41.0	−41.8	−41	−41.3	−46.2	−40.9	−40.0	−34.3	−41.8
	mean	−36.3	−34.2	−39.0	−31.8	−40.1	−39.5	−39.2	−40.3	−40.8	−42.1	−38.5	−38.5	−33.5	−37.6
	sd	6.3	0.9	7.6	16.7	2.5	1.3	1.8	0.4	0.6	4.4	2.2	1.3	1.1	5.9
	max	−27.5	−32.7	−29.5	−1.8	−37.0	−37.0	−37	−40	−40	−37.5	−36.3	−37.0	−32.7	−33.5
d-excess (‰)	min	12.2	10.0	13.4	8.9	10.5	9.6	10.1	10.6	9.3	10.7	8.7	10.5	15.8	12.0
	mean	14.0	11.9	15.4	12.7	11.8	10.8	11.4	11.5	11.2	12.7	9.2	11.7	16.3	13.9
	sd	1.0	0.9	1.9	2.5	0.8	0.9	1.4	0.6	1.0	3.0	0.6	1.4	0.8	2.8
	max	15.6	13.7	19.8	16.7	12.6	12.2	13.7	12.4	12.2	16.1	10.0	13.7	16.9	15.9

Table 2. Statistical table of physico-chemical parameters, major ions, and isotope of water samples (ionic form).

Parameter	2020–2022					2015–2016					2009–2013				
	Code	RL-SIF	RL-VAS	REG-1	PLRL	RL-SIF	RL-VAS	RL1	RL2	RL3	RL-SIF	RL-VAS	RL1	RL2	RL3
	<i>n</i>	7	8	8	/	7	9	5	9	/	3	4	/	/	/
T (°C)	min	10.2	10.8	3.9	/	9.2	11.4	/	/	/	9.2	11.4	/	/	/
	mean	11.1	12.3	10.1	/	11.7	12.9	/	/	/	10.9	12.4	/	/	/
	sd	0.8	0.7	4.8	/	1.1	0.6	/	/	/	1.6	0.7	/	/	/
	max	12.4	13.2	19.9	/	13.3	13.5	/	/	/	12.3	12.9	/	/	/
pH	min	7.9	8.1	7.6	/	7.6	7.9	/	/	/	8.1	8.3	/	/	/
	mean	8.1	8.3	8.1	/	8.0	8.2	/	/	/	8.1	8.3	/	/	/
	sd	0.1	0.1	2.6	/	0.2	0.2	/	/	/	0	0	/	/	/
	max	8.2	8.4	8.4	/	8.2	8.4	/	/	/	8.2	8.4	/	/	/
EC ($\mu\text{S}/\text{cm}$ at 25 °C)	min	154	322	111	/	143	290	/	/	/	143	357	/	/	/
	mean	182	391	156	/	175	387	/	/	/	162	393	/	/	/
	sd	25	39	32	/	24	40	/	/	/	31	40	/	/	/
	max	244	454	224	/	204	444	/	/	/	198	444	/	/	/
HCO_3^- hydrogencarbonate (mg/L)	min	73.2	207.5	47.0	/	76.3	195.0	142.0	142.0	/	75.1	140.3	/	/	/
	mean	94.1	258.0	75.4	/	95.4	254.8	148.0	150.0	/	90.7	230.7	/	/	/
	sd	23.9	30.2	17.1	/	14.4	30.5	4.0	5.0	/	27.1	62.7	/	/	/
	max	140.3	294.7	103.7	/	114.0	289.0	154.0	159.0	/	122.0	273.4	/	/	/
Cl^- chloride (1-) (mg/L)	min	5.9	5.3	4.9	/	4.9	5.1	3.9	4.1	/	5.3	0.9	/	/	/
	mean	6.9	5.8	5.6	/	5.9	5.4	4.4	4.7	/	5.8	5.4	/	/	/
	sd	1.0	0.6	0.6	/	0.9	0.2	0.5	0.3	/	0.7	3.1	/	/	/
	max	8.6	7.2	6.4	/	7.6	5.6	5.1	5.0	/	6.5	7.6	/	/	/
SO_4^{2-} tetraoxidosulfate (2-) (mg/L)	min	4.0	5.0	3.1	/	4.2	4.9	1.0	1.0	/	4.8	1.7	/	/	/
	mean	4.9	6.1	5.0	/	5.7	6.2	1.3	1.1	/	6.2	7.8	/	/	/
	sd	1.2	0.9	1.3	/	0.8	0.6	0.2	0.1	/	2.1	4.7	/	/	/
	max	7.4	7.6	7.0	/	6.5	7.1	1.6	1.3	/	8.7	12.9	/	/	/
NO_3^- trioxidonitrate (1-) (mg/L)	min	0.6	0.4	0.1	/	2.0	1.0	2.2	3.7	/	1.2	1.2	/	/	/
	mean	1.7	0.7	0.3	/	2.8	1.3	2.4	4.4	/	1.8	1.2	/	/	/
	sd	1.0	0.2	0.1	/	0.7	0.1	0.1	0.4	/	0.7	0	/	/	/
	max	3.5	0.9	0.4	/	3.9	1.4	2.5	4.8	/	2.6	1.2	/	/	/
Na^+ sodium (1+) (mg/L)	min	3.3	3.1	2.7	/	3.2	3.4	2.7	3.2	/	3.5	0.8	/	/	/
	mean	3.8	3.3	3.2	/	4.4	3.7	2.9	3.7	/	3.9	3.4	/	/	/
	sd	0.5	0.2	0.3	/	0.9	0.4	0.1	0.7	/	0.7	1.7	/	/	/
	max	4.6	3.6	3.5	/	5.8	4.6	3.0	5.6	/	4.7	4.5	/	/	/
K^+ potassium (1+) (mg/L)	min	0.5	0.3	0.1	/	0.4	0.3	0.1	0.1	/	0.3	0.1	/	/	/
	mean	1.1	0.7	0.2	/	0.9	0.4	0.1	0.1	/	0.4	0.3	/	/	/
	sd	0.4	0.6	0.0	/	0.4	0.1	0.0	0.0	/	0.1	0.1	/	/	/
	max	1.4	2.2	0.3	/	1.6	0.5	0.1	0.1	/	0.5	0.5	/	/	/

Table 2. Cont.

Parameter	Code	2020–2022				2015–2016					2009–2013				
		RL-SIF	RL-VAS	REG-1	PLRL	RL-SIF	RL-VAS	RL1	RL2	RL3	RL-SIF	RL-VAS	RL1	RL2	RL3
		<i>n</i>	7	8	8	/	7	9	5	9	/	3	4	/	/
Ca ²⁺ calcium (2+) (mg/L)	min	16.0	29.0	11.6	/	16.8	22.8	25.7	24.6	/	16.1	29.1	/	/	/
	mean	17.8	37.2	18.0	/	19.4	35.8	26.8	26.5	/	18.3	35.4	/	/	/
	sd	1.5	5.6	3.8	/	1.3	7.4	0.7	0.9	/	2.1	6.5	/	/	/
	max	20.4	43.9	22.5	/	20.7	43.5	27.6	27.5	/	20.1	43.2	/	/	/
Mg ²⁺ magnesium (2+) (mg/L)	min	6.4	28.1	3.7	/	6.0	26.7	12.6	14.0	/	6	29.2	/	/	/
	mean	9.3	30.2	4.9	/	9.0	30.8	13.6	14.6	/	8.4	31.6	/	/	/
	sd	3.1	1.2	0.9	/	2.3	2.4	0.7	0.5	/	3.7	2.9	/	/	/
	max	15.0	31.8	6.1	/	12.1	34.9	14.4	15.2	/	12.7	35	/	/	/
	n	13	17	10	17	7	9	5	9	7	3	4	2	2	2
δ ¹⁸ O oxygen-18 (‰)	min	−8.21	−6.01	−35.95	−9.68	−6.85	−6.65	−6.49	−6.63	−6.67	−7.11	−6.29	−6.46	−6.26	−6.72
	mean	−6.29	−5.77	−34.95	−5.56	−6.49	−6.28	−6.32	−6.47	−6.5	−6.85	−5.96	−6.28	−6.23	−6.45
	sd	0.88	0.12	0.69	2.20	0.29	0.18	0.23	0.09	0.15	0.23	0.28	0.25	0.04	0.39
	max	−5.03	−5.55	−34.00	−1.75	−6.08	−6.08	−5.94	−6.32	−6.32	−6.70	−5.63	−5.94	−6.20	−6.17
δ ² H deuterium (‰)	min	−50.1	−36.0	−52.6	−62.9	−43.7	−41.0	−41.8	−41	−41.3	−46.2	−40.9	−40.0	−34.3	−41.8
	mean	−36.3	−34.2	−39.0	−31.8	−40.1	−39.5	−39.2	−40.3	−40.8	−42.1	−38.5	−38.5	−33.5	−37.6
	sd	6.3	0.9	7.6	16.7	2.5	1.3	1.8	0.4	0.6	4.4	2.2	1.3	1.1	5.9
	max	−27.5	−32.7	−29.5	−1.8	−37.0	−37.0	−37	−40	−40	−37.5	−36.3	−37.0	−32.7	−33.5
d-excess (‰)	min	12.2	10.0	13.4	8.9	10.5	9.6	10.1	10.6	9.3	10.7	8.7	10.5	15.8	12.0
	mean	14.0	11.9	15.4	12.7	11.8	10.8	11.4	11.5	11.2	12.7	9.2	11.7	16.3	13.9
	sd	1.0	0.9	1.9	2.5	0.8	0.9	1.4	0.6	1.0	3.0	0.6	1.4	0.8	2.8
	max	15.6	13.7	19.8	16.7	12.6	12.2	13.7	12.4	12.2	16.1	10.0	13.7	16.9	15.9

The hydrograph, thermograph, chemograph (HTC) δ¹⁸O, and Mg/Ca ratio of the cave sump and Regolo Creek waters, the flow rate measures of the Regolo Creek, and the 15 min mean precipitation amount in the studied area are reported in Figure 4. The 15 min mean precipitation amount was calculated by averaging the pluviometric data taken from two meteorological stations (Canevara—TOS02004011 and Vergheto—TOS02000047; Figure 1a) of the Regional Hydrologic Service (<http://www.sir.toscana.it/pluviometria-pub> (accessed on 1 May 2022)).

The HTC-graph shows a typical karst system regime [51] characterized by sharp increases in the water level in the cave sump, with a very short response time, to heavy precipitations. The water level peaks occurred after a few hours from the meteoric events, and after those, the system quickly returned to pre-event conditions (one up to three days). At the cave sump, the highest water levels were reached during February, April–May, and September–December 2021, up to 600 cm H₂O, due to abundant long-lasting precipitation with possible snow melt contributions, especially during spring. The flow rates measured in the Regolo Creek were in accordance with both the precipitation pattern and the water level variation in the cave sump, reaching the highest values (105 and 110 L/s on 30 April and 29 January 2021, respectively) after heavy and/or long-lasting precipitations, and the lowest values (2 and 20 L/s on 31 and 1 March 2021, respectively) when precipitations were scarce or absent. From September to December 2021, the pattern was characterized by sharp increases in the water level and almost undisturbed recession phases. These peaks were related to intense but short-time rainfall events. The summer of 2021 was marked by weak and sporadic precipitation, leading to a significant decrease in the water level until dry conditions were reached. The water level fluctuations were accompanied by the T and EC oscillations. Both parameters showed different patterns with the highest mean values occurring in March 2021 and September 2021 for the EC, and from September to November 2021 for the T. Lower values lasted during May and from September to December 2021. The EC significantly decreased from about 230 μS/cm to roughly 130 μS/cm after the strongest precipitations. During precipitation events, the EC showed a significant variation (up to −100 μS/cm when the system was very dry), quickly decreasing when the water level peaks occurred, whereas the T did not always show the same pattern. Such behavior is unusual, since the temperature normally decreases due to the infiltration of meteoric and stream waters, which also normally results in a marked lowering of the EC [52]. The δ¹⁸O patterns of the cave sump and Regolo Creek waters were very similar, characterized by an

enrichment in heavy isotopes due to the seasonal and amount effect during spring 2021. The $\delta^{18}\text{O}$ isotopic composition of RL-TOR, a water sample collected on 30 April 2021 from a tiny water flow inside the cave that was not active during other monitoring campaigns, was -5.68% , very close to the $\delta^{18}\text{O}$ isotopic values of the cave sump and Regolo Creek samples collected during the same campaign (-5.59% and -5.66% for RL-SIF and REG-1, respectively). The Mg/Ca ratio was almost constant for the Regolo Creek, ranging from 0.44 to 0.46 mmol/L, whereas the Mg/Ca ratio of the cave sump varied as a function of the precipitation rates with the lowest values after heavy and/or long-lasting precipitations (0.60 and 0.63 mmol/L on 29 January and 30 April 2021, respectively) and had the highest value when scarce or no precipitation occurred (1.17 mmol/L on 1 March 2021).

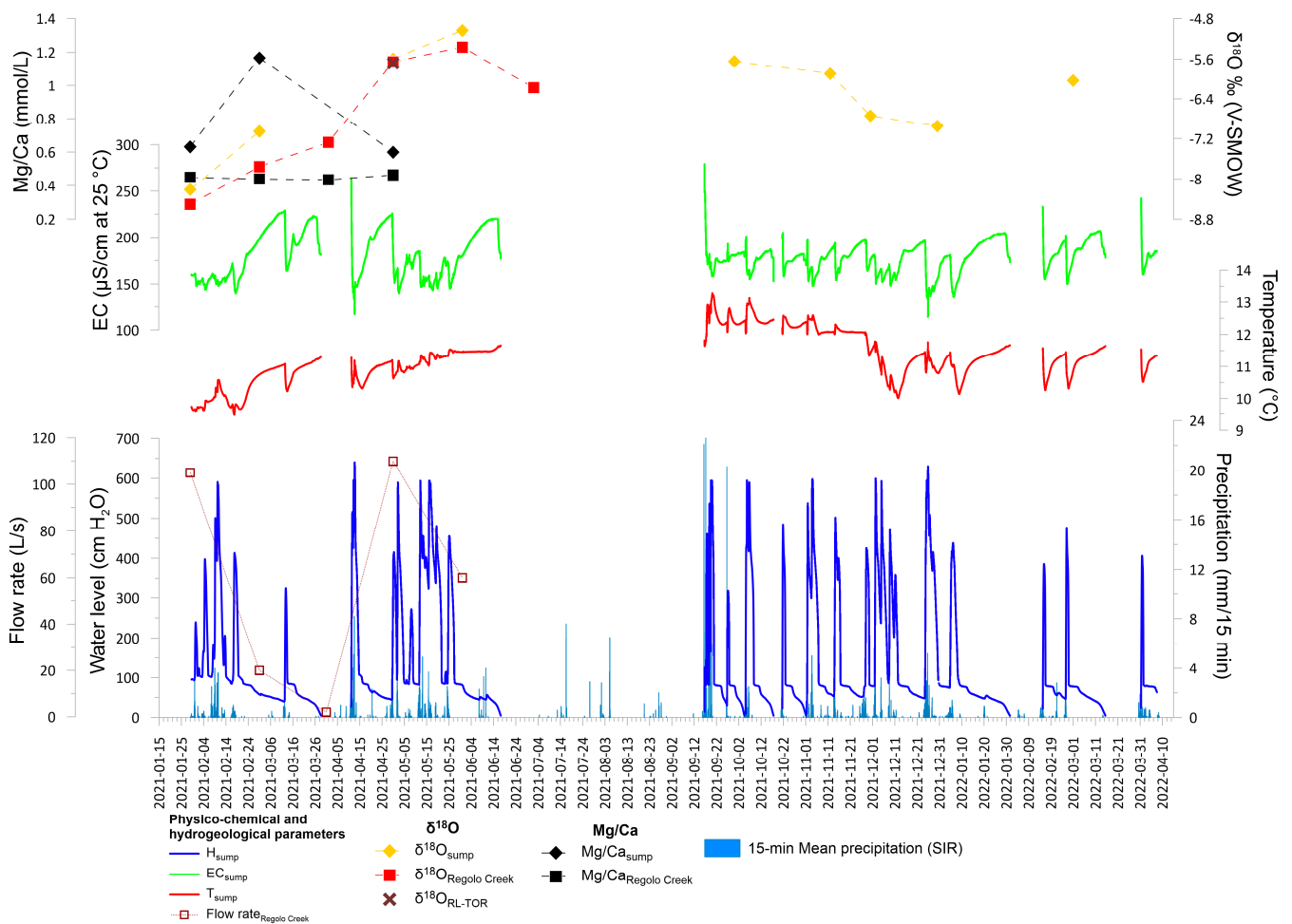


Figure 4. HTC-graph, $\delta^{18}\text{O}$, and Mg/Ca ratio of the cave sump related to 15 min mean precipitation amount in the studied area from 29 January 2021 to 7 April 2022. Red lined squares: $\delta^{18}\text{O}$ of the Regolo Creek. Dark red pointed squares: Regolo Creek flow rate. Black lined squares: Mg/Ca ratio of the Regolo Creek. Brown cross: $\delta^{18}\text{O}$ of RL-TOR sample.

The summary statistics of the major chemical elements and isotopic variables for each sampling point are reported in Tables 1 and 2. The hydrochemistry data are given in the Supplementary Materials (SM—Table S1). The identification of the hydrochemical facies of the waters was performed by plotting the results of the analysis for each sample on a Piper-Hill diagram [53]; Figure 5a. Two main hydrochemical facies were recognized.

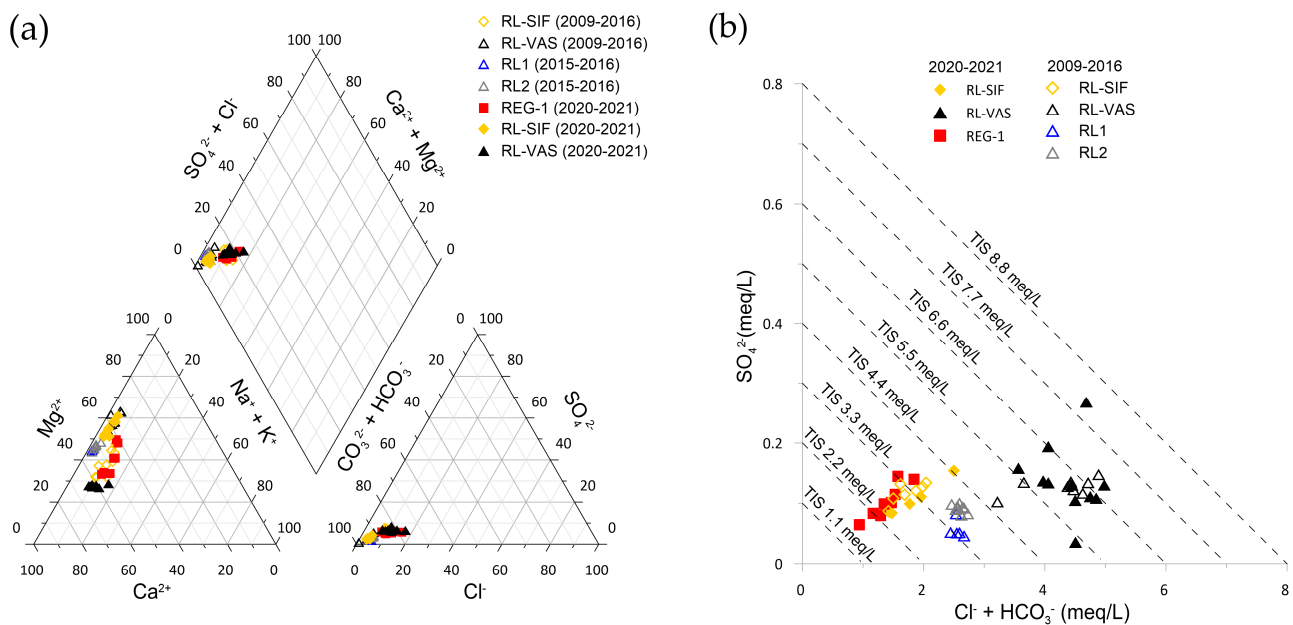


Figure 5. (a) Piper-Hill classification diagram of stream and cave waters. (b) $\text{HCO}_3^- + \text{Cl}^-$ vs. SO_4^{2-} diagram of stream and cave waters (TIS, total ionic salinity).

Ca-HCO_3 is the hydrochemical facies most representative of the Regolo Creek samples, and partially of the sump. The dominant anion is HCO_3^- . The percentages of $\text{Na}^+ + \text{K}^+$ in the Regolo Creek waters were higher if compared to those measured in the sump and drip pool (percentages between 9 and 12.5%).

Ca-Mg-HCO_3 is the predominant hydrochemical facies in the drip pool waters. The main anion is HCO_3^- . The Mg^{2+} content was always above 50%, up to percentage values close to 70% of the total concentration of cations in the solution. The Na^+ and K^+ content were less than 5%. The RL1 and RL2 drips also showed a Ca-Mg-HCO_3 composition, but in contrast to the drip pool, the Mg^{2+} content was slightly lower and equal, in percentage, to the Ca^{2+} content. During some sampling, the sump also showed an enrichment in Mg^{2+} with a trend moving to a Ca-Mg-HCO_3 composition.

The drip waters and the drip pool differ from the sump and the Regolo Creek stream waters by higher bicarbonate, Ca^{2+} , and Mg^{2+} concentrations. These data agree with the highest EC values measured in the drip pool and the highest TIS (total ionic salinity) values (5.5 to 7.0 meq/L) (Figure 5b). The drip waters showed TIS values close to 4.0 meq/L for RL2 and RL3, and slightly lower for RL1 (around 3.5 meq/L). The sump and Regolo Creek waters, on the other hand, generally showed lower TIS values, ranging from 1.8 to 3.4 meq/L, except for the sump sample collected in September 2020, which had a higher salinity (4.5 meq/L). In general, the TIS is quite variable in the different sampling campaigns for the sump, drip pool, and Regolo Creek waters, whereas the drip waters' TIS is almost stable throughout the monitoring period. The NO_3^- and SO_4^{2-} content were very low for all sampling periods.

4.3. Isotopic Composition of Precipitation, Stream, and Cave Waters

The isotope data of the precipitation, stream, and cave water samples collected during different monitoring can be found in the Supplementary Materials (SM—Table S1), and the statistics are given in Tables 1 and 2. The isotope data of the local precipitation, stream, and cave waters are displayed in the typical $\delta^2\text{H}$ vs. $\delta^{18}\text{O}$ diagram, along with five different meteoric water lines (MWLs, Figure 6) which were useful for understanding the origin of the investigated waters.

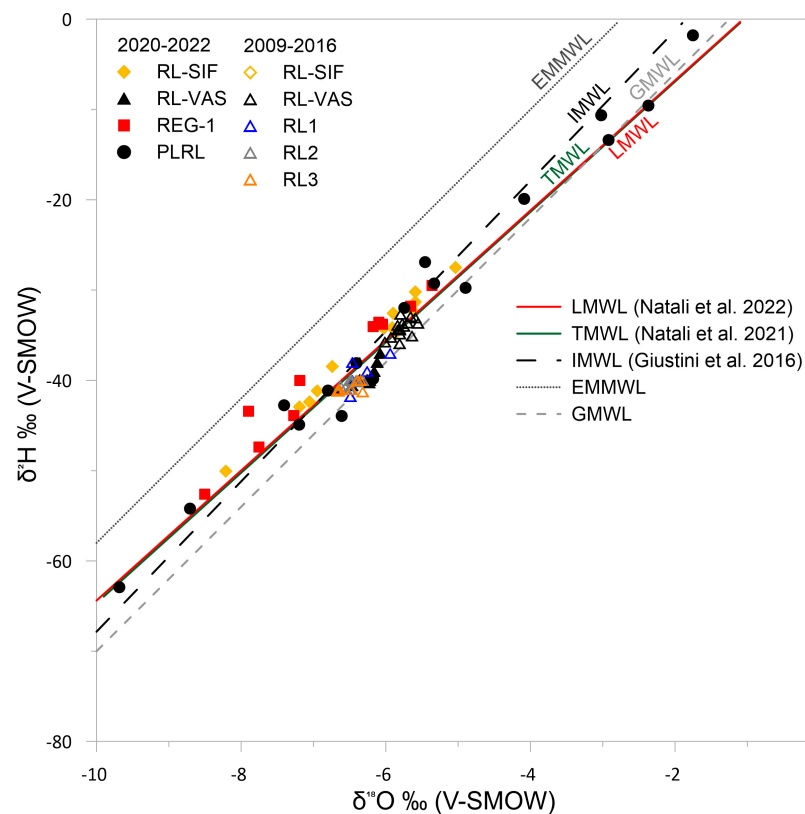


Figure 6. $\delta^2\text{H}$ – $\delta^{18}\text{O}$ diagram of stream, cave waters, and local precipitations [37,54,55].

As observed in this diagram, the local monthly precipitations collected over the monitoring period were characterized by a high isotope variability, with the isotopic values ranging from a minimum of -9.68‰ for $\delta^{18}\text{O}$ and -62.9‰ for $\delta^2\text{H}$ recorded in January 2021 to a maximum of -1.75‰ and -1.8‰ in March 2021, respectively, for $\delta^{18}\text{O}$ and $\delta^2\text{H}$. The amount-weighted mean isotopic composition of precipitation was -6.16‰ for $\delta^{18}\text{O}$ and -35.6‰ for $\delta^2\text{H}$, and was depleted in heavy isotopes compared with its mean ($-5.56 \pm 2.20\text{‰}$ for $\delta^{18}\text{O}$ and $-31.8 \pm 16.6\text{‰}$ for $\delta^2\text{H}$). The Regolo Creek and cave waters were distributed close to the Tuscany Meteoric Water Line TMWL [54], IMWL [55], and LMWL in the Apuan Alps area as calculated for the monthly precipitation collected at PLRL from November 2020 to August 2021 [37], confirming their origin by the infiltration of local precipitations.

As expected, both the stream and cave waters were characterized by a much narrower range of $\delta^{18}\text{O}$ and $\delta^2\text{H}$ values if compared to the precipitation. The RL2 and RL3 drips and the drip pool presented the lowest isotopic variability, while the RL1 showed a larger isotope variability. The isotopic composition of the oxygen and hydrogen of the cave sump and the Regolo Creek water samples was rather variable, characterized by a high standard deviation compared to their mean value ($-6.42 \pm 0.70\text{‰}$ and $-6.80 \pm 1.1\text{‰}$ for $\delta^{18}\text{O}$, $-38.2 \pm 5.5\text{‰}$ and $-39.0 \pm 7.6\text{‰}$ for $\delta^2\text{H}$, respectively), but lower with respect to the precipitation. The mean isotopic composition calculated for the drip pool waters was $-5.95 \pm 0.28\text{‰}$ for $\delta^{18}\text{O}$ and $-36.4 \pm 2.8\text{‰}$ for $\delta^2\text{H}$, and it was rather similar to the amount-weighted mean precipitation composition. The mean oxygen and hydrogen isotopic values of the RL2 ($-6.43 \pm 0.13\text{‰}$ for $\delta^{18}\text{O}$ and $-39.1 \pm 2.8\text{‰}$ for $\delta^2\text{H}$) and RL3 ($-6.49 \pm 0.19\text{‰}$ for $\delta^{18}\text{O}$ and $-40.1 \pm 2.5\text{‰}$ for $\delta^2\text{H}$) drips were depleted in heavy isotopes if compared to the amount-weighted mean isotope composition of precipitation and showed no significant differences between them. The mean isotopic composition of the RL1 drip ($-6.35 \pm 0.21\text{‰}$ for $\delta^{18}\text{O}$ and $-38.8 \pm 2.7\text{‰}$ for $\delta^2\text{H}$) was also depleted in heavy isotopes if compared to the precipitation, but it was characterized by a larger variability than the other two drips.

Most of the water samples tended to have a more negative isotopic composition compared to the weighted average precipitation. Both the summer and low precipitations,

which were generally more positive, played a minor role in the recharge; indeed, the isotopic signal of the cave and stream waters were mostly distributed along more negative values, which were more representative of the winter, autumn, and spring precipitations.

The isotopic monitoring of the precipitation, cave sump, Regolo Creek, and drip pool has permitted the recording of the isotopic variability over time, which is useful for tracking the current hydrologic processes. As shown in Figure 7, a marked isotopic depletion was registered in the stream and sump waters in winter 2020–2021, starting from December 2020, as a consequence of high precipitation isotopically depleted. As a matter of fact, the isotopic changes registered in the stream and sump waters closely reflect the isotopic variations in the precipitation, which showed more negative values in December 2020 and January 2021. Thereafter, the precipitation became more enriched in heavy isotopes, and the sump and Regolo Creek waters also showed the same pattern until the isotopic values of the latter tends to stabilize at slightly more enriched values. Starting from September 2021, the isotopic composition of the sump waters tends to negativize again as a result of heavy rainfall. The isotopic composition of the drip pool was almost steady during the entire monitoring period, characterized by an enrichment in $\delta^{18}\text{O}$ content with respect to the $\delta^{18}\text{O}$ amount-weighted mean of precipitations.

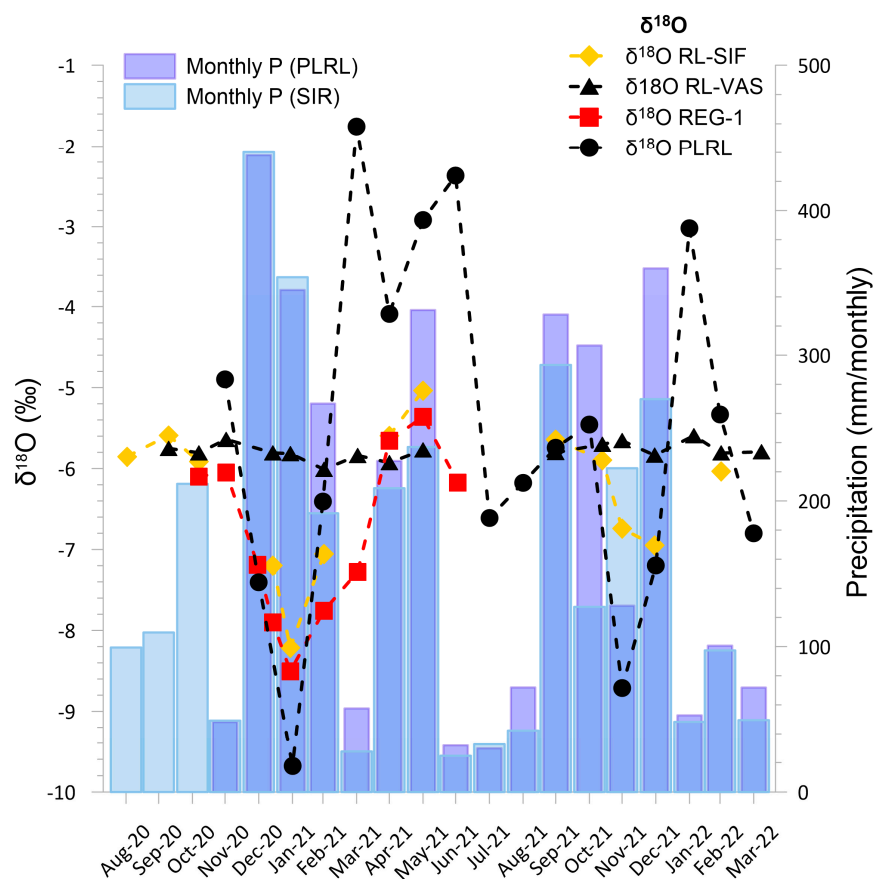


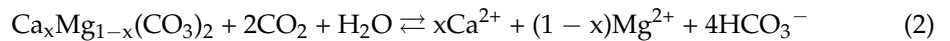
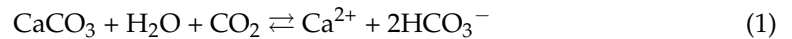
Figure 7. Time plot of $\delta^{18}\text{O}$ values of the cave sump (RL-SIF), drip pool (RL-VAS), Regolo Creek (REG-1) waters, and local precipitations (PLRL) collected from September 2020 to April 2022. Monthly precipitations (SIR) are calculated by averaging monthly pluviometric data taken from two meteorological stations (Canevara—TOS02004011 and Vergheto—TOS02000047) of the Regional Hydrologic Service.

5. Discussion

5.1. Hydrochemical Processes: Carbonate Dissolution, Dilution, and Calcite Precipitation

The results of the chemical analyses conducted on the water samples, in agreement with Piper-Hill's diagram, indicated that the chemistry of the cave waters was essentially

determined by the dissolution processes of the carbonate lithotypes present in the investigated area and the dilution processes that occurred as a result of intense events. According to formulae (1) and (2), the dissolution of carbonate (calcite and/or dolomite), which produced Ca-HCO₃ or Ca-Mg-HCO₃ waters, was the predominant process in the study area.



The different content of HCO₃⁻, Ca²⁺, and Mg²⁺ in the collected samples depends substantially on the water residence time, the intensity of the water-rock interaction processes, and the amount and frequency of precipitation.

As shown in the binary diagram of Ca + Mg vs. HCO₃ (Figure 8a), the cave and stream water samples were displayed along the 1:1 line, evidencing that the dissolution of calcite and/or dolomite was the predominant reaction in the groundwater system. The Mg²⁺ + Ca²⁺ and HCO₃⁻ concentrations of the different samples highlighted how these waters were characterized by distinct degrees of maturity. The cave sump and Regolo Creek waters showed the largest compositional variability and were the least mature; the gradual decrease in the ionic content of these waters when heavy and/or prolonged precipitations occurred suggested dilution. The drip waters were the least variable in terms of ionic content, and they were more enriched in Mg²⁺ + Ca²⁺ and HCO₃⁻ due to more intense and prolonged water-rock interaction processes, also promoted by lower water-rock ratios and longer residence times within the soil as well as in the epikarst. At last, the drip pool waters were characterized by the highest ionic content and exhibit a certain compositional variability, probably related to the calcite and/or dolomite precipitation from oversaturated solutions (samples with Mg²⁺ > Ca²⁺). Longer residence times of waters feeding the drip pool can lead to incongruent dissolution phenomena, whereby the waters acquire larger amounts of Mg²⁺ depending on the different solubility of calcite and dolomite [40].

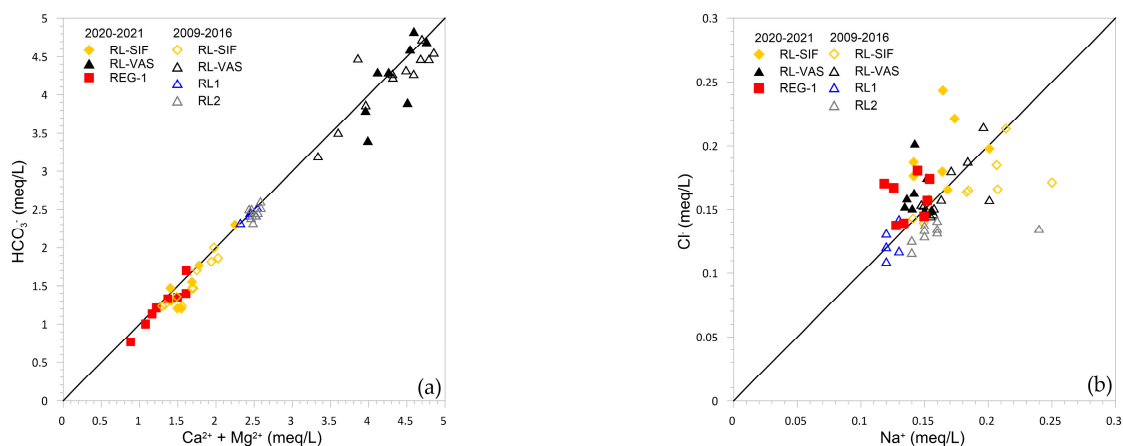


Figure 8. Binary diagrams for water samples. The black lines correspond to the 1:1 ratio. (a) Ca²⁺ + Mg²⁺ vs. HCO₃⁻. (b) Na⁺ vs. Cl⁻.

All waters were characterized by low sodium and chloride contents, generally close to the stoichiometric 1:1 ratio, as shown in Figure 8b, demonstrating that their origin was mainly attributable to marine chloride wet and dry deposition [56,57].

5.2. Isotope Hydrogeochemistry of Drip Pool and Drip Waters and Relation with Precipitation

The drip pool waters collected from September 2020 to April 2022 were enriched in heavy isotopes compared to the weighted mean isotopic composition of local precipitation (Figure 9a), as a consequence of possible equilibrium fractionations. The variations in the isotopic content did not temporally follow the local precipitation pattern, demonstrating

that the drip pool was the expression of a karst circuit that allowed the precipitation to homogenize isotopically during infiltration. The isotopic composition of the drip pool, RL2, and RL3 drips collected during the 2015–2016 monitoring campaign (Figure 9b) was almost constant, and they exhibited a similar pattern characterized by more negative isotopic values for drips, which was probably due to their shorter residence times and shortest circulation in the karst system; the stationarity of the isotopic composition suggested the presence of a karst circuit that allowed isotopic homogenization of the infiltration waters that supplied them. The RL1 drip, on the other hand, showed a more pronounced temporal variability due to its shallower position, resulting in a quicker response to the precipitations that did not allow the isotopic homogenization of the infiltration waters.

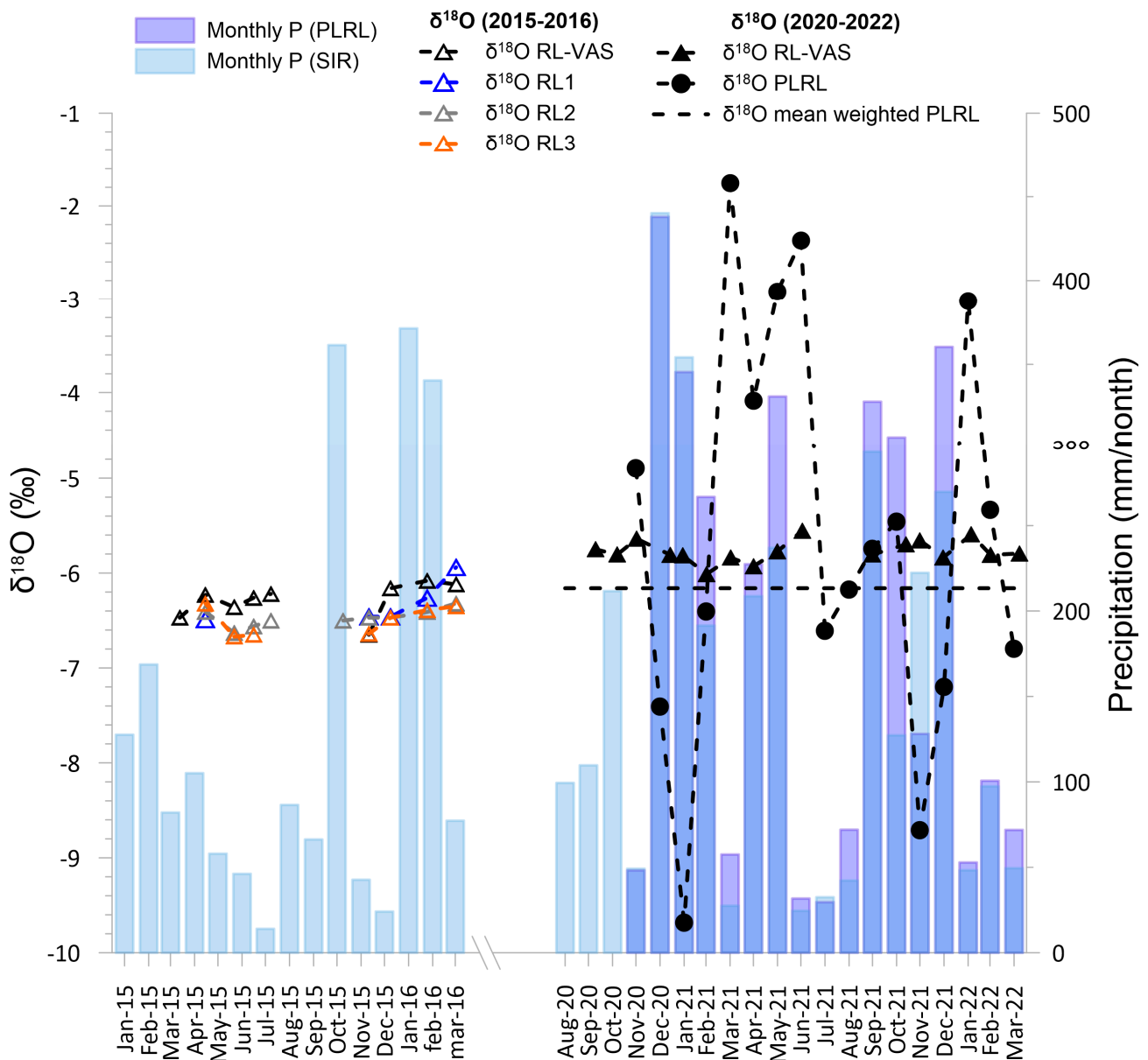


Figure 9. $\delta^{18}\text{O}$ time plot of the drip pool (RL-VAS), drips (RL1, RL2, RL3), and local precipitation (PLRL) related to monthly precipitations from March 2015 to March 2016, and from September 2020 to March 2022. Monthly P (SIR) are calculated by averaging monthly pluviometric data taken from two meteorological stations (Canevara—TOS02004011 and Vergheto—TOS02000047) of the Regional Hydrologic Service.

5.3. Cave Sump Water Sources: Hydrology, Hydrogeochemistry, and Its Relationship with Regolo Creek

As shown in the HTC-graph (Figure 4), the sump exhibited a typical karst hydrodynamic regime [51]. The sharp rises in the water level in response to significant meteorological events, followed by a relatively quick return (usually within 2–3 days) to pre-event conditions indicates elevated hydraulic conductivity of the karst system. The residual rise in the water level that persisted after the peaks was tiny in comparison with the peaks values and tended to decrease in a relatively short time. These hydrodynamic characteristics and the presence of a complex karst system upstream of the Renella Cave suggested that the cave sump is probably an occasional overflow of the local karst aquifer that is partially supplied by the Regolo Creek and its tributaries. A possible minor contribution due to the direct infiltration of local precipitation cannot be ruled out, given the high permeability by the fracturing and karstification of the rocks outcropping in the area, combined with the presence of a quarry area above the cave. The discharge peaks measured in the Regolo Creek on 29 January and 30 April 2021 were both in agreement with the very low EC values and the very high water level measured in the sump on 30 April 2021 (over 400 cm H₂O). The minimum EC values were the result of the strong dilution related to the potential inflow of waters from the local karst aquifer into the cave sump when heavy precipitations occurred. The maximum EC values were probably the consequence of different co-occurring phenomena. When the system was very dry, the Regolo Creek stream waters, that partially supply the local karst aquifer, were more mature as a result of longer water–rock interactions. Additionally, as the waters entered the karst circulation system, they became enriched as a result of possible mixing with the waters from small pools presented within the cave, which were much more concentrated in anions and cations due to prolonged interaction with the surrounding rocks. The variability of the Mg/Ca ratio and isotopic composition of the cave sump and Regolo Creek waters as a function of the precipitation pattern were both in agreement with the hydrodynamic, physico-chemical, and flow rate data, suggesting that the cave sump responded rather rapidly to the precipitations, likely through the inflow of the Regolo Creek diluted waters during the flood stages, characterized by lower values of Mg/Ca ratio and a minimum difference in the isotopic composition, that were also consistent with the isotopic composition of RL-TOR.

6. Conclusions

In this article, the monthly monitoring of the Renella Cave karst system is resumed, attempting to hydrochemically and isotopically characterize cave waters and understand as much as possible the hydrology of the system, the relations that exist with local precipitations and the Regolo Creek stream waters, and with the surrounding hydrogeological system. The aim is to provide a dataset to better understand the climatic signal present in different geochemical proxies and to reconstruct the hydrological relations existing between the cave sump and the karst system recharges, given the importance of the Apuan Alps in terms of groundwater resources.

The classification based on the Piper-Hill diagram indicated that both the Regolo Creek and cave waters belong to the bicarbonate-alkaline earth hydrochemical facies, indicating that their chemism is essentially determined by the dissolution of the Grezzoni Fm.

As shown in the Ca-Mg-HCO₃ plot, there were differences in the chemism of stream and cave waters. The Regolo Creek and the cave sump waters were strongly influenced by the amount of local precipitations. The lower interaction of the cave sump waters with carbonate rocks, which were mainly derived from the contribution of the local aquifer and Regolo Creek waters during the flood stages, resulted in their low maturity and their predominantly bicarbonate-calcic chemism. The contribution of the Regolo Creek waters to the cave sump was also highlighted by the EC and T patterns measured by the CTD-Diver, which showed rapid fluctuations depending on the amount of local precipitations, whereas the water level rises in the cave sump could not be directly linked to an increase in the flow rate until the overflow threshold was exceeded.

The drips and drip pool were supplied by waters that come from a slower karst circuit, so depending on the duration and intensity of the water–rock interaction processes, they were more mature and enriched in ions. The low concentrations of Na^+ and Cl^- in the stream and groundwater samples were presumably due to the contribution of wet and dry deposition by marine aerosols; in contrast, the contribution of the marine component to the total value of Ca^{2+} and Mg^{2+} concentrations was almost zero.

A correlation between the local precipitation patterns and temporal variation in the isotopic composition of the waters was observed. The lower variability of $\delta^{18}\text{O}$ and $\delta^2\text{H}$ values measured in the drips and drip pool samples would indicate that their supplies were related to a longer karst circuit that permitted meteoric waters to homogenize isotopically during infiltration. The more variable isotopic values measured in the cave sump and Regolo Creek samples, on the other hand, suggested a short infiltration time and a direct connection with meteoric events that did not allow the waters to homogenize isotopically.

Further research is required to confirm the presence of a circulation network fragmented into independent parts and to make considerations about the residence and infiltration times of meteoric waters. It would be interesting for future research to carry on the monitoring of local precipitations, stream, and cave waters in order to obtain a multi-year framework of the hydrochemical and isotopic variability of these waters, and highlight the sensitivity of the site to the precipitation seasonality.

Therefore, the study of this karst system and the data given and processed in this paper could be a good starting point to begin an activity aimed to carry out detailed hydrogeological reconstructions.

Supplementary Materials: The following supporting information can be downloaded at <https://www.mdpi.com/article/10.3390/w15091764/s1>, Table S1: physico-chemical parameters, hydrochemistry, and isotopes data of precipitation, stream, and cave waters.

Author Contributions: Conceptualization, M.C., S.N. and G.Z.; methodology, M.C., S.N. and G.Z.; software, M.C. and S.N.; validation, M.C., S.N., G.Z., I.B., I.I., R.G., M.D. and L.P.; formal analysis, M.C. and S.N.; investigation, M.C., S.N., G.Z., I.B., I.I. and M.D.; resources, S.N., G.Z., I.B., M.D. and R.G.; data curation, M.C., S.N., G.Z., I.B. and M.D.; writing—original draft preparation, M.C.; writing—review and editing, M.C., S.N., G.Z., I.B., I.I., M.D., R.G. and L.P.; visualization, M.C. and S.N.; supervision, S.N. and G.Z.; project administration, G.Z.; funding acquisition, G.Z. and R.G. All authors have read and agreed to the published version of the manuscript.

Funding: This research was funded by the Politecnico di Torino UGOV 579999_2019_ZANCHE TTA_POLITECNICO_TORINO and UGOV 579999_2010_GIANNECCHINI.

Data Availability Statement: The precipitation data are available at the website of the Regional Hydrological Service of Tuscany (<https://www.sir.toscana.it/consistenza-rete>, accessed on 1 May 2022). The hydrochemistry and isotopic data are not readily available because they will be used for other publications. Requests to access the dataset should be directed to the corresponding authors.

Acknowledgments: The authors are indebted to the technicians of the Institute of Geosciences and Earth Resources of Pisa (CNR-IGG) and the Laboratory of Fluid Geochemistry of the University of Florence for their support in the laboratory analysis.

Conflicts of Interest: The authors declare no conflict of interest. The funders had no role in the design of the study; in the collection, analyses, or interpretation of data; in the writing of the manuscript; or in the decision to publish the results.

References

1. Hamza, M.H.; Added, A.; Rodríguez, R.; Abdeljaoued, S.; Ben Mammou, A. A GIS-based DRASTIC vulnerability and net recharge reassessment in an aquifer of a semi-arid region (Metline-Ras Jebel-Raf Raf aquifer, Northern Tunisia). *J. Environ. Manag.* **2007**, *84*, 12–19. [[CrossRef](#)]
2. Andreo, B.; Vías, J.; Durán, J.J.; Jiménez, P.; López-Get, J.A.; Carrasco, F. Methodology for groundwater recharge assessment in carbonate aquifers: Application to pilot sites in southern Spain. *Hydrogeol. J.* **2008**, *16*, 911–925. [[CrossRef](#)]
3. Chenoweth, J.; Hadjikakou, M.; Zoumides, C. Quantifying the human impact on water resources: A critical review of the water footprint concept. *Hydrol. Earth Syst. Sci.* **2014**, *18*, 2325–2342. [[CrossRef](#)]

4. Doveri, M.; Piccini, L.; Menichini, M. Hydrodynamic and geochemical features of metamorphic carbonate aquifers and implications for water management: The Apuan Alps (NW Tuscany-Italy) case study. In *Karst Water Environment*; Younos, T., Schreiber, M., Kosić Ficco, K., Eds.; Springer International Publishing: Cham, Switzerland, 2019; pp. 209–249. [CrossRef]
5. Marić, N.; Matić, I.; Papić, P.; Beškoski, V.P.; Ilić, M.; Gojgić-Cvijović, G.; Miletić, S.; Nikić, Z.; Vrvić, M.M. Natural attenuation of petroleum hydrocarbons—A study of biodegradation effects in groundwater (Vitanovac, Serbia). *Environ. Monit. Assess* **2018**, *190*, 89. [CrossRef]
6. Ford, D.; Williams, P.D. *Karst Hydrogeology and Geomorphology*; John Wiley & Sons: Chichester, UK, 2007.
7. Pu, J.; Cao, M.; Zhang, Y.; Yuan, D.; Zhao, H. Hydrochemical indications of human impact on karst groundwater in a subtropical karst area. Chongqing, China. *Environ. Earth Sci.* **2014**, *72*, 1683–1695. [CrossRef]
8. Iván, V.; Mádl-Szőnyi, J. State of the art of karst vulnerability assessment: Overview, evaluation and outlook. *Environ. Earth Sci.* **2017**, *76*, 112. [CrossRef]
9. Liang, Y.; Zhao, C.; Tang, C.; Shen, H.; Wang, Z.; Gao, X.; Wang, Y. Characterization, evolution, and environmental issues of karst water systems in Northern China. *Hydrogeol. J.* **2018**, *26*, 1371–1385. [CrossRef]
10. Stevanović, Z. Karst waters in potable water supply: A global scale overview. *Environ. Earth Sci.* **2019**, *78*, 662. [CrossRef]
11. Goldscheider, N.; Chen, Z.; Auler, A.S.; Bakalowicz, M.; Broda, S.; Drew, D.; Hartmann, J.; Jiang, G.; Moosdorf, N.; Stevanovic, Z.; et al. Global distribution of carbonate rocks and karst water resources. *Hydrogeol. J.* **2020**, *28*, 1661–1677. [CrossRef]
12. Olarinoye, T.; Gleeson, T.; Marx, V.; Seeger, S.; Adinehvand, R.; Allocca, V.; Andreo, B.; Apaéstegui, J.; Apolit, C.; Arfib, B.; et al. Global karst springs hydrograph dataset for research and management of the world’s fastest-flowing groundwater. *Sci. Data* **2020**, *7*, 59. [CrossRef] [PubMed]
13. Tedd, K.M.C.; Coxon, E.; Misstear, B.D.R.; Daly, D.; Craig, M.; Mannix, A.; Hunter Williams, N.H. An integrated pressure and pathway approach to the spatial analysis of groundwater nitrate: A case study from the southeast of Ireland. *Sci. Total Environ.* **2014**, *476*, 460–476. [CrossRef]
14. Bates, B.C.; Kundzewicz, Z.; Wu, S.; Palutikof, J. (Eds.) *Climate Change and Water*; Technical Paper of the Intergovernmental Panel on Climate Change; IPCC Secretariat: Geneva, Switzerland, 2008; p. 210. Available online: <http://www.taccire.sua.ac.tz/handle/123456789/552> (accessed on 10 April 2023).
15. Giorgi, F. Thirty years of regional climate modeling: Where are we and where are we going next? *J. Geophys. Res. Atmos.* **2019**, *124*, 5696–5723. [CrossRef]
16. Worthington, S. Characteristics of channel networks in unconfined carbonate aquifers. *GSA Bulletin* **2014**, *127*, 759–769. [CrossRef]
17. Patekar, M.; Bašić, M.; Pola, M.; Kosović, I.; Terzić, J.; Lucca, A.; Mittempergher, S.; Berio, L.R.; Borović, S. Multidisciplinary investigations of a karst reservoir for managed aquifer recharge applications on the island of Vis (Croatia). *Acque Sotter. Ital. J. Groundw.* **2022**, *11*, 37–48. [CrossRef]
18. Kazakis, N.; Chalikakis, K.; Mazzilli, N.; Ollivier, C.; Manakos, A.; Voudouris, K. Management and research strategies of karst aquifers in Greece: Literature overview and exemplification based on hydrodynamic modelling and vulnerability assessment of a strategic karst aquifer. *Sci. Total Environ.* **2018**, *643*, 592–609. [CrossRef]
19. Goldscheider, N.; Drew, D. Speleological investigations. *Int. J. Speleol.* **2008**, *37*, 27–40. [CrossRef]
20. Hartmann, A.; Lange, J.; Weiler, M.; Arbel, Y.; Greenbaum, N. A new approach to model the spatial and temporal variability of recharge to karst aquifers. *Hydrol. Earth Syst. Sci.* **2012**, *16*, 2219–2231. [CrossRef]
21. Perrin, J.; Jeannin, P.Y.; Zwahler, F. Epikarst storage in a karst aquifer: A conceptual model based on isotopic data. Milandre test site, Switzerland. *J. Hydrol.* **2003**, *279*, 106–124. [CrossRef]
22. Aquilina, L.; Ladouche, B.; Dörfliger, N. Water storage and transfer in the epikarst of karstic systems during high flow periods. *J. Hydrol.* **2006**, *327*, 472–485. [CrossRef]
23. Williams, P.W. The role of the epikarst in karst and cave hydrogeology: A review. *Int. J. Speleol.* **2008**, *37*, 1–10. [CrossRef]
24. Drysdale, R.N.; Zanchetta, G.; Hellstrom, J.C.; Fallick, A.E.; Zhao, J.X.; Isola, I.; Bruschi, G. Palaeoclimatic implications of the growth history and stable isotope ($\delta^{18}\text{O}$ and $\delta^{13}\text{C}$) geochemistry of a middle to late Pleistocene stalagmite from central-western Italy. *Earth Planet Sci. Lett.* **2004**, *227*, 215–229. [CrossRef]
25. Drysdale, R.N.; Zanchetta, G.; Hellstrom, J.; Maas, R.; Fallick, A.; Pickett, M.; Cartwright, I.; Piccini, L. Late Holocene drought responsible for the collapse of Old World civilizations is recorded in an Italian cave flowstone. *Geology* **2006**, *34*, 101–104. [CrossRef]
26. Isola, I.; Zanchetta, G.; Drysdale, R.N.; Regattieri, E.; Bini, M.; Bajo, P.; Hellstrom, J.C.; Baneschi, I.; Lionello, P.; Woodhead, J.; et al. The 4.2 ka event in the central Mediterranean: New data from a Corchia speleothem (Apuan Alps; central Italy). *Clim. Past* **2019**, *15*, 135–151. [CrossRef]
27. Zanchetta, G.; Regattieri, E.; Isola, I.; Drysdale, R.N.; Bini, M.; Baneschi, I.; Hellstrom, J.C. The so-called “4.2 Event” in the Central Mediterranean and its climatic teleconnections. *Alp. Mediterr. Quat.* **2016**, *29*, 5–17.
28. Zanchetta, G.; Bini, M.; Bloomfield, K.; Izdebski, A.; Vivoli, N.; Regattieri, E.; Isola, I.; Drysdale, R.N.; Bajo, P.; Hellstrom, J.C.; et al. Beyond one-way determinism: San Frediano’s miracle and climate change in Central and Northern Italy in late antiquity. *Clim. Chang.* **2021**, *165*, 25. [CrossRef]
29. Zhorniyak, L.V.; Zanchetta, G.; Drysdale, R.N.; Hellstrom, J.C.; Isola, I.; Regattieri, E.; Piccini, L.; Baneschi, I.; Couchoud, I. Stratigraphic evidence for a “pluvial phase” between ca 8200–7100 ka from Renella cave (Central Italy). *Quat. Sci. Rev.* **2011**, *30*, 409–417. [CrossRef]

30. Piccini, L.; Pranzini, G.; Tedici, L.; Forti, P. Le risorse idriche dei complessi carbonatici del comprensorio Apuo-Versiliese. *Quad. Geo. App.* **1999**, *6*, 61–78.
31. Piccini, L. Acquiferi carbonatici e sorgenti carsiche delle Alpi Apuane. In Proceedings of the Le Risorse Idriche Sotterranee Delle Alpi Apuane: Conoscenze Attuali e Prospettive di Utilizzo: Massa, Italy, 22 June 2002; pp. 41–76.
32. Piccini, L.; Di Lorenzo, T.; Costagliola, P.; Galassi, D.M.P. Marble Slurry's Impact on Groundwater: The Case Study of the Apuan Alps Karst Aquifers. *Water* **2019**, *11*, 2462. [[CrossRef](#)]
33. Köppen, W. *Grundriss der Klimakunde*; de Gruyter: Berlin, Germany; Boston, MA, USA, 1931. [[CrossRef](#)]
34. Lionello, P.; Bhend, J.; Buzzi, A.; Della-Marta, P.M.; Krichak, S.O.; Jansà, A.; Maheras, P.; Sanna, A.; Trigo, R. Cyclones in the Mediterranean region. Climatology and effects on the environment. In *Developments in Earth and Environmental Sciences*; Elsevier: Amsterdam, The Netherlands, 2006; Volume 4, pp. 325–372. [[CrossRef](#)]
35. Reale, M.; Lionello, P. Synoptic climatology of winter intense precipitation events along the Mediterranean coasts. *Nat. Hazards Earth Syst. Sci.* **2013**, *13*, 1707–1722. [[CrossRef](#)]
36. Trigo, I.F.; Bigg, G.R.; Davies, T.D. Climatology of cyclogenesis mechanisms in the Mediterranean. *Am. Meteorol. Soc.* **2002**, *130*, 549–569. [[CrossRef](#)]
37. Natali, S.; Doveri, M.; Giannecchini, R.; Baneschi, I.; Zanchetta, G. Is the deuterium excess in precipitation a reliable tracer of moisture sources and water resources fate in the western Mediterranean? New insights from Apuan Alps (Italy). *J. Hydrol.* **2022**, *614*, 128497. [[CrossRef](#)]
38. López-Moreno, J.I.; Vicente-Serrano, S.M.; Morán-Tejada, E.; Lorenzo-Lacruz, J.; Kenawya, A.; Beniston, M. Effects of the North Atlantic Oscillation (NAO) on combined temperature and precipitation winter modes in the Mediterranean mountains: Observed relationships and projections for the 21st century. *Glob. Planet Ch.* **2011**, *77*, 62–76. [[CrossRef](#)]
39. Luppichini, M.; Barstanti, M.; Giannecchini, R.; Bini, M. Statistical relationships between large-scale circulation patterns and local-scale effects: NAO and rainfall regime in a key area of the Mediterranean basin. *Atmos. Res.* **2021**, *248*, 105270. [[CrossRef](#)]
40. Piccini, L.; Zanchetta, G.; Drysdale, R.N.; Hellstrom, J.; Isola, I.; Fallick, A.E.; Leone, G.; Doveri, M.; Mussi, M.; Mantelli, F.; et al. The environmental features of the Monte Corchia cave system (Apuan Alps, central Italy) and their effects on speleothem growth. *Int. J. Speleol.* **2008**, *37*, 153–172. [[CrossRef](#)]
41. Natali, S. Idrologia e Idrochimica del Sistema Carsico Buca della Renella (Forno, Massa): Implicazioni Paleoambientali. Bachelor's Thesis, University of Pisa, Pisa, Italy, 2015.
42. Tardelli, A. Studio idrologico e idrochimico del sistema carsico Buca della Renella (Forno, Massa-Carrara): Implicazioni paleoambientali. Master's Thesis, University of Pisa, Pisa, Italy, 2016.
43. Moore, R.D. Introduction to Salt Dilution Gauging for Streamflow Measurement Part 2: Constant-rate Injection. *Watershed Manag. Bull.* **2004**, *8*, 1.
44. Østrem, Gunnar A method of measuring water discharge in turbulent streams. *Geogr. Bull.* **1964**, *21*, 21–43.
45. Appelo, C.A.J.; Postma, D. *Geochemistry, Groundwater and Pollution*, 2nd ed.; Appelo, C.A.J., Postma, D., Eds.; CRC Press: Boca Raton, FL, USA, 2005. [[CrossRef](#)]
46. Epstein, S.; Mayeda, T. Variation of ^{18}O content of waters from natural sources. *Geochim. Cosmochim. Acta* **1953**, *4*, 213–224. [[CrossRef](#)]
47. Lis, G.; Wassenaar, L.I.; Hendry, M.J. High-Precision Laser Spectroscopy D/H and $^{18}\text{O}/^{16}\text{O}$ Measurements of Microliter Natural Water Samples. *Anal. Chem.* **2008**, *80*, 287–293. [[CrossRef](#)]
48. Craig, H. Standards for reporting concentrations of deuterium and ^{18}O in natural waters. *Science* **1961**, *133*, 1833–1834. [[CrossRef](#)]
49. Baneschi, I.; Piccini, L.; Regattieri, E.; Isola, I.; Guidi, M.; Lotti, L.; Mantelli, F.; Menichetti, M.; Drysdale, R.N.; Zanchetta, G. Hypogean microclimatology and hydrology of the 800–900 m a.s.l. level in the Monte Corchia cave (Tuscany, Italy): Preliminary considerations and implications for paleoclimatological studies. *Acta Carsologica* **2011**, *40*, 175–187. [[CrossRef](#)]
50. Regattieri, E.; Zanchetta, G.; Drysdale, R.N.; Isola, I.; Hellstrom, J.; Roncioni, A. A continuous stable isotopic record from Penultimate glacial maximum on to the Last Interglacial (159–121 ka) from Tana Che Urla Cave (Apuan Alps, central Italy). *Quat. Res.* **2014**, *82*, 450–461. [[CrossRef](#)]
51. Petrič, M.; Kogovšek, J. Hydrogeological Characteristics of the Area of Intermittent Karst Lakes of Pivka. *Acta Carsologica* **2005**, *34*, 599–618. [[CrossRef](#)]
52. Piccini, L.; Nannoni, A.; Poggetti, E. Hydrodynamics of karst aquifers in metamorphic carbonate rocks: Results from spring monitoring in the Apuan Alps (Tuscany, Italy). *Hydrogeol. J.* **2023**, *31*, 241–255. [[CrossRef](#)]
53. Piper, A.M. A graphic procedure in the geochemical interpretation of water analyses. *Eos. Trans. AGU* **1944**, *25*, 914–928. [[CrossRef](#)]
54. Natali, S.; Baneschi, I.; Doveri, M.; Giannecchini, R.; Selmo, E.; Zanchetta, G. Meteorological and geographical control on stable isotopic signature of precipitation in a western Mediterranean area (Tuscany, Italy): Disentangling a complex signal. *J. Hydrol.* **2021**, *603*, 126944. [[CrossRef](#)]
55. Giustini, F.; Brilli, M.; Patera, A. Mapping oxygen stable isotopes of precipitation in Italy. *J. Hydrol. Reg. Stud.* **2016**, *8*, 162–181. [[CrossRef](#)]

56. Guan, H.; Love, A.J.; Simmons, C.T.; Makhnin, O.; Kayaalp, A.S. Factors influencing chloride deposition in a coastal hilly area and application to chloride deposition mapping. *Hydrol. Earth Syst. Sci.* **2010**, *14*, 801–813. [[CrossRef](#)]
57. Mantelli, F.; Lotti, L.; Montigiani, A.; Piccini, L. Chimica delle acque del Complesso Carsico del Monte Corchia. *Acta Apuana* **2015**, *11*, 33–45.

Disclaimer/Publisher’s Note: The statements, opinions and data contained in all publications are solely those of the individual author(s) and contributor(s) and not of MDPI and/or the editor(s). MDPI and/or the editor(s) disclaim responsibility for any injury to people or property resulting from any ideas, methods, instructions or products referred to in the content.